2011

High resolution regional seismic attenuation tomography in eastern Tibetan Plateau and adjacent regions

Xueyang Bao

Eric Sandvol

See next page for additional authors

Citation/Publisher Attribution

Bao, X., E. Sandvol, J. Ni, T. Hearn, Y. J. Chen, and Y. Shen (2011), High resolution regional seismic attenuation tomography in eastern Tibetan Plateau and adjacent regions, *Geophys. Res. Lett.*, 38, L16304, doi: 10.1029/2011GL048012.
Available at: https://doi.org/10.1029/2011GL048012

High resolution regional seismic attenuation tomography in eastern Tibetan Plateau and adjacent regions

Xueyang Bao,[1] Eric Sandvol,[1] James Ni,[2] Thomas Hearn,[2] Yongshun John Chen,[3] and Yang Shen[4]

Received 3 May 2011; revised 14 July 2011; accepted 14 July 2011; published 18 August 2011.

[1] The Q of regional seismic phases *Lg* and *Pg* within the crust is assumed as a proxy for crustal Q_β and Q_α, which is used as a constraint of crustal rheology. We measure regional-phase Q of the eastern Tibetan Plateau and adjacent areas. This method eliminates contributions from source and site responses and is an improvement on the Two-Station Method (TSM). We have generated tomographic images of crustal attenuation anomalies with resolution as high as 1°. In general we observe low Q in the northernmost portions of the Tibetan Plateau and high Q in the more tectonically stable regions such as the interior of the Qaidam basin. The calculated site responses appear to correlate with topography or sediment thickness. Furthermore the relationship between earthquake magnitudes and calculated source terms suggest that the RTM method effectively removes the source response and may be used as an alternative to source magnitude.
Citation: Bao, X., E. Sandvol, J. Ni, T. Hearn, Y. J. Chen, and Y. Shen (2011), High resolution regional seismic attenuation tomography in eastern Tibetan Plateau and adjacent regions, *Geophys. Res. Lett.*, *38*, L16304, doi:10.1029/2011GL048012.

1. Introduction

[2] *Lg* is typically a prominent high-frequency seismic phase at regional distances traveling in the continental crust. The measurement of *Lg* attenuation, typically described by a frequency dependent quality factor Q_{Lg}, has been suggested as an approximation for Q_β of the crust [*Mitchell*, 1995]. Thus Q_{Lg} could be used to interpret crustal temperature and rheology. The spatial and temporal variation of crustal heating and melting in the TP is an essential element in nearly all geodynamic models for plateau uplift [*McKenzie and Priestley*, 2008]. An important but often ignored measure of the present day thermal state of the TP crust is its high frequency seismic attenuation properties. There have been numerous studies of *Lg* attenuation in Tibet and adjacent areas over the last three decades, most of which obtain high attenuation throughout the TP [e.g., *McNamara et al.*, 1996; *Reese et al.*, 1999; *Phillips et al.*, 2000; *Xie*, 2002; *Fan and Lay*, 2003]. Unfortunately, many of these studies have obtained inconsistent results, probably because they were obtained with different methods and databases. In this study, we apply a Reverse Two-station/event Method (RTM) [*Chun et al.*, 1987] in eastern Tibetan Plateau using seismic records from several newly deployed seismic networks that nearly cover the entire eastern half of the TP. This method has been suggested to be very accurate [*Ford et al.*, 2008] and can greatly improve existing models of crustal attenuation in this area.

2. Method

[3] The RTM is a significant improvement upon the Two-Station Method (TSM) [*Xie and Mitchell*, 1990]. The TSM assumes that the variation in site responses is negligible. Previous studies, however, have suggested that the site effects are non-unique, nonlinear, and frequency-dependent, as well as possessing strong lateral variations [e.g., *Jemberie and Langston*, 2005]. The RTM avoids the effects of site response variation and inaccurate instrument responses. Figure S1 in the auxiliary material shows the geometry of the RTM including its two cases: the Reverse Two Station (RTS) paths and Reverse Two Event (RTE) paths.[1] The RTM Q_{Lg} can be calculated as:

$$\frac{1}{Q_{Lg}} = \frac{V_{Lg}}{\pi f\left(d_{aj} + d_{bi} - d_{ai} - d_{bj}\right)} \ln\left[\frac{A_{ai}A_{bj}}{A_{aj}A_{bi}}\left(\frac{d_{ai}d_{bj}}{d_{aj}d_{bi}}\right)^m\right], \quad (1)$$

where A_{ai}, A_{aj}, A_{bi}, A_{bj} denote spectral amplitude of Lg recorded at stations i and j for events a and b, d_{ai}, d_{aj}, d_{bi}, d_{bj} the corresponding distances, f the frequency, m the geometrical spreading coefficient (0.5 in frequency domain), and V_{Lg} the group velocity of *Lg* (about 3.5 km/s). We obtain the Q_{Lg} from (1) by solving a linear regression problem in the frequency domain. The case of RTE has the advantage to fill in the area devoid of station, which increases the utility of the RTM, and can become effective in constructing models in areas that are seismically active but without dense seismic networks.

[4] The inter-station site response difference can also be solved by using the RTM:

$$\ln\frac{SS_i}{SS_j} = \ln\frac{I_j}{I_i} + \frac{d_{aj} - d_{ai}}{d_{aj} + d_{bi} - d_{ai} - d_{bj}} \ln\frac{A_{ai}d_{ai}^m}{A_{aj}d_{aj}^m} + \frac{d_{bi} - d_{bj}}{d_{aj} + d_{bi} - d_{ai} - d_{bj}} \ln\frac{A_{bi}d_{bi}^m}{A_{bj}d_{bj}^m}. \quad (2)$$

[1]Department of Geological Sciences, University of Missouri, Columbia, Missouri, USA.
[2]Department of Physics, New Mexico State University, Las Cruces, New Mexico, USA.
[3]Institute of Theoretical and Applied Geophysics, School of Earth and Space Sciences, Peking University, Beijing, China.
[4]Graduate School of Oceanography, University of Rhode Island, Narragansett, Rhode Island, USA.

0094-8276/11/2011GL048012

[1]Auxiliary materials are available in the HTML. doi:10.1029/2011GL048012.

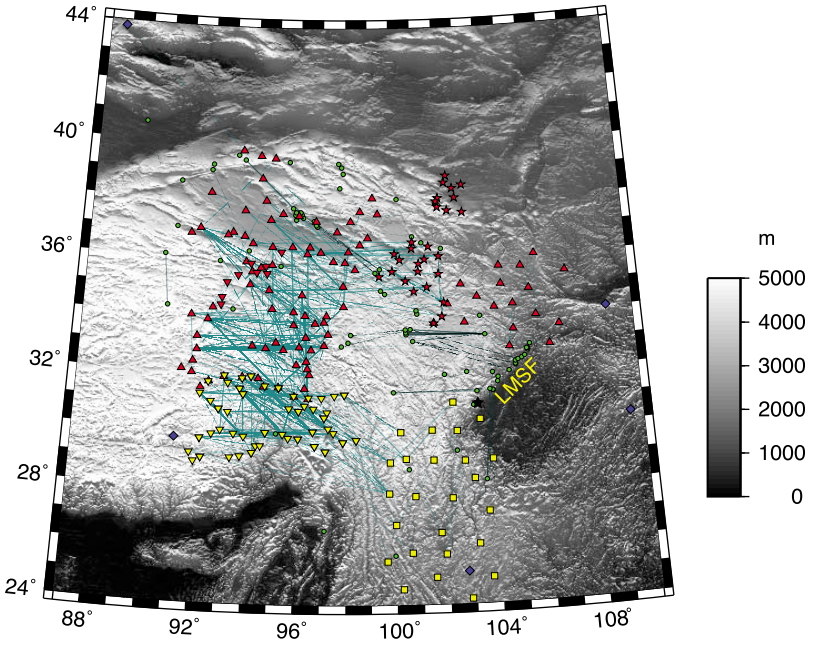

Figure 1. Map showing seismic stations, regional seismic events, and two-station or two-event paths in this study. The yellow inverse triangles represent Namche Barwa experiment; the yellow squares represent MIT-China experiment; the red triangles represent INDEPTH-IV-ASCENT experiment; the red inverse triangles represent INDEPTH-IV-UK experiment; the red stars represent NETS experiment; the blue diamonds represent the permanent network IC; the green circles represent events. The cyan and black lines represent RTS and RTE paths at 1 Hz, respectively. The epicenter of the Mw 7.9 Wenchuan earthquake is marked by black star, and the Longmenshan Fault (LMSF) area is noted. Elevation is shown with a gray scale.

A similar problem to (2) was discussed by *Moya and Irikura* [2003]. We apply an LSQR algorithm [*Paige and Saunders*, 1982] to calculate the lateral variation in relative site responses for each station. The relative values of source excitation function (S) can be obtained using a similar method. The S has been modeled as a function of seismic moment M_0 [*Brune*, 1970], which can be estimated from earthquake moment magnitude [*Hanks and Kanamori*, 1979]. This suggests that the S derived from the RTM can be used to infer the source magnitude.

3. Data Collection and Processing

[5] The data analyzed in this study are waveforms recorded at 6 permanent broadband seismic stations from New China Digital Seismograph Network (CDSN) and 217 temporary broadband seismic stations from Namche Barwa Tibet, MIT-China, ASCENT, INDEPTH-IV-UK, and part of Northern Tibet Plateau Seismic Experiment (NETS). All stations are within or around the TP and provide a nearly complete coverage of the eastern TP. Waveform data from 779 regional events taken from the Preliminary Determination of Epicenters catalog (PDE) from the U. S. Geological Survey (USGS) and the China Seimic Network (CSN) catalog were used in this study (Figure 1). We limit the epicentral distances to greater than 3°, the hypocentral depths to less than the Moho using the crustal thickness model of *Shin et al.* [2007], and magnitudes (M_L) to equal or less than 7 to avoid complicated source functions.

[6] We use the method of *Xie* [2002] in cutting *Lg* windows and calculating *Lg* spectral amplitude. In total, 18266 *Lg* spectra are calculated and compared with the pre-*Pn* noise spectra by setting a minimum signal-noise ratio of 2 to minimize the influence of ambient noise. We calculate RTM Q_{Lg} values at discrete frequencies of 0.5 Hz, 1 Hz, and 2 Hz. To select the reverse paths, we set criteria that the maximum difference for all azimuthal angles ($\delta\theta_a$, $\delta\theta_b$, $\delta\theta_i$, and $\delta\theta_j$ in Figures S1b and S1d) is ±15°, the minimum inter-station/event distance for d_{ij} and d_{ab} is 150 km, and only paths with standard errors of less than 50% in measuring Q_{Lg} are used. Although the amount of RTS paths is much larger than that of RTE paths, the RTE measurements are important in areas without RTS path coverage, especially along the Longmenshan Fault (LMSF) which benefits from an extremely dense aftershock sequence that occurred after the Mw 7.9 Wenchuan earthquake (Figure 1). The measured Q_{Lg} values are subsequently used to map the lateral variations of Q_{Lg} at selected frequencies using an LSQR algorithm. Resolution tests (Figure S3) using 2-D checkerboard anomaly patterns and ±15% random noise at different cell sizes and different frequencies show relatively good resolution at scales of 1° × 1° and 2° × 2° within most of the study area. We discretize the study area into 0.5° × 0.5° cells and obtain tomographic maps of Q_{Lg} at frequencies of 0.5 Hz, 1 Hz, and 2 Hz (Figure S4).

4. Result and Discussion

[7] The eastern TP and adjacent regions involved in this study are tectonically divided into a number of terranes that may correlate with strong variations in crustal properties [e.g., *Klemperer*, 2006]. The Lhasa Block, Qiangtang Terrane, and Songpan-Ganzi fold belt (SGFB) compose the majority of TP from south to north. The Longmenshan thrust belt, probably

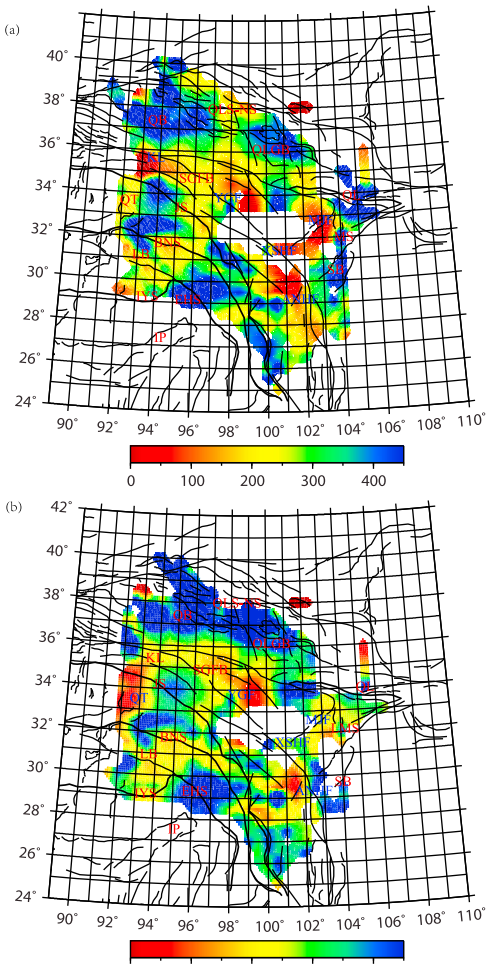

Figure 2. (a) Q_{Lg} and (b) Q_{Pg} tomographic images at 1 Hz. Thick lines represent tectonic sutures, and thin lines represent faults. ANHF: Anninghe Fault; BNS: Bangong-Nujiang Suture; EHS: Eastern Himalayan Syntaxis; IP: Indian Plate; IYS: Indus-Yalu Suture; JS: Jinsha Suture; KL: Kunlun mountain belt; LB: Lhasa Block; LMS: Longmenshan mountain belt; MJF: Minjiang Fault; QB: Qaidam Basin; QLGB: Qinghai Lake-Gonghe Basin; QL: Qinling mountain belt; QLS-NS: Qilian Shan-Nan Shan Mountain belt; QT: Qiangtang Terrane; SB: Sichuan Basin; SGFB: Songpan-Ganzi fold belt; XSHF: Xianshuihe Fault; YGF: Yushu-Ganzi Fault.

initiated in late Miocene to early Pliocene, separates the eastern TP and the Sichuan Basin. This area also includes the Qaidam Basin, the Qilian Shan-Nan Shan, and the Qinling mountain belt. The Q_{Lg} tomographic maps at different frequencies show significant lateral variations but the pattern of the variation is not strongly frequency dependent. Thus Q_{Lg0} (Q_{Lg} at 1 Hz) map (Figure 2a) mainly reflects the major *Lg* attenuation structure of the study area. The Q_{Lg0} values in this map can be divided into four ranges: low ($Q_{Lg0} < 150$), low to middle ($150 < Q_{Lg0} < 250$), middle to high ($250 < Q_{Lg0} < 350$), and high ($Q_{Lg0} > 350$). The northeastern TP that lies north and east of the Jinsha Suture has widespread low to middle Q_{Lg0} values. High Q_{Lg0} values are observed in the Sichuan Basin, Qaidam Basin, and Qinghai Lake-Gonghe Basin. A high Q_{Lg0} zone is located within the Eastern Himalayan Syntaxis (EHS) and probably extends eastward to the Bangong-Nujiang Suture in the southern TP. Along the Kunlun Mountains, we observe an low Q_{Lg0} "band" divides the Qaidam Basin and central TP. Another low Q_{Lg0} zone, approximately along the western Longmenshan thrust belt, divides the Sichuan Basin and eastern TP. An average Q_{Lg0} of 366 measured by *McNamara et al.* [1996] is within the range of Q_{Lg0} values (100~400) in the same area of our model. The low Q_{Lg0} values estimated by *Xie* [2002] and *Fan and Lay* [2003] for the northern TP are also similar with our result. And our model shows a very similar pattern of lateral variation Q_{Lg0} with the result of *Phillips et al.* [2000].

[8] A complex velocity structure may lead to scattering attenuation and regional phase mode conversion when *Lg* propagates in a strongly heterogeneous crust [e.g., *Kennett*, 1989]. But a large number of studies imply that the Q_{Lg} is a good estimation for crustal shear wave Q_β, and the scattering only plays a minor role and is probably negligible at

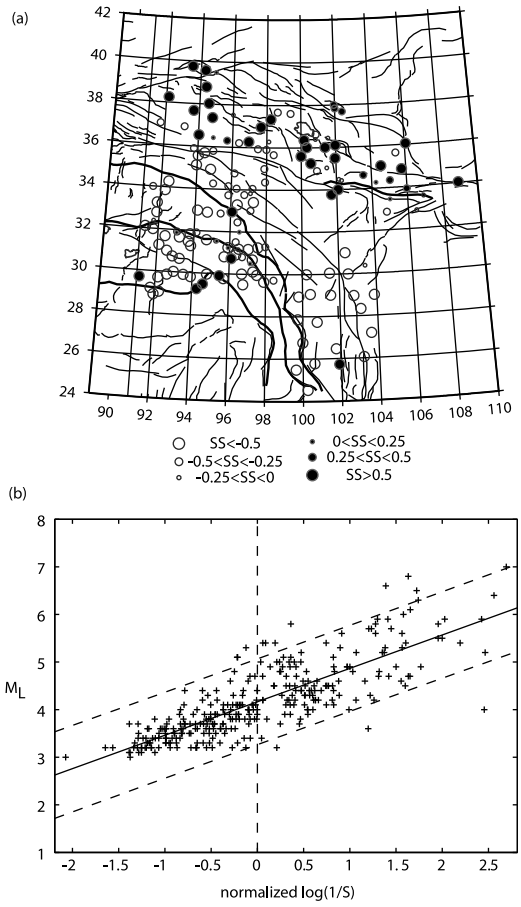

Figure 3. (a) *Lg* site response maps at frequencies of 1 Hz. Here *SS* represents the site response of each station relative to the average of site responses within the whole area. We observe significant site response difference between the Tibetan Plateau and major basins, probably due to topography or sedimentary thickness. (b) A nearly linear relationship is observed between logarithm of the reciprocal of normalized source term (solved from *Lg* RTM at 1 Hz) and magnitude M_L. The solid line represents the least-square linear fit line and the two dashed lines parallel to it represent its 95% confidence interval. It indicates that the source term solved from *Lg* amplitude using RTM is well correlated with seismic magnitude M_L when $3 \le M_L \le 7$.

low frequencies [e.g., *Mitchell*, 1995]. We only measure *Lg* at frequencies around 1 Hz in our study, which is similar to the frequency ranges used in previous studies referenced above. As a result, the lateral variation of Q_{Lg} should largely represent the lateral variation of crustal Q_β, and should help us to infer variations in geothermal structures.

[9] We observe of high Q_{Lg0} in the Qaidam Basin and Sichuan Basin with tectonically stable crust and low temperatures. The high Q_{Lg0} zone in the EHS may be related to the underthrusting Indian Plate. The low Q_{Lg} band along the Kunlun Mountains within the SGFB correlates with a suggested low velocity zone (LVZ) in the middle to lower crust [e.g., *Yang et al.*, 2010] and the high strain rate in this region [*Holt et al.*, 2000]. This correlation suggests a connection between high strain rate, LVZ, and high seismic attenuation in the crust. Strain heating has been suggested as a mechanism for high temperature and partial melting in convergent orogens [*Nabelek et al.*, 2010]. The crust of northern TP is probably dry and hot [*Hacker et al.*, 2000]. If the low Q_{Lg} along the Kunlun Mountains is caused by a hot crust, the high temperature and low viscosity crust (within the northwestern SGFB) may be caused by the high strain rate. The low Q_{Lg} zone approximately along the eastern margin of TP also correlates with middle to lower crustal LVZ from recent observation [*Li et al.*, 2010], but whether these two low Q_{Lg} bands are connected is still unknown in our model because of no path coverage near the center of the SGFB.

[10] The site responses have a strong spatial structure across the TP (Figure 3a). We consistently observe high site responses within the Qaidam Basin and low site responses within the TP at different frequencies (Figure S5). The lateral variation does not correlate with either the difference in instrument response (Figure S2) or the Vs30 model in this area [*Wald and Allen*, 2007] (the global Vs30 model is available at http://earthquake.usgs.gov/hazards/apps/vs30/custom.php). Alternatively, it is possible that the site response strongly varies with the change in topography. Meanwhile, the site response may be affected by near-surface geological structures [*Su et al.*, 1992]. Our result of high site responses within the Qaidam Basin, who has widespread sediment thicker than 10 km, suggests that thick sedimentary basins probably enhance the site amplification.

[11] In terms of our source terms, we observe a nearly linear relationship between the logarithm of the reciprocal of normalized source term and earthquake magnitude M_L (Figure 3b) when $3 \le M_L \le 7$. This correlation is expected if a constant stress drop model is assumed [*Reese et al.*, 1999]. Our result suggests that *Lg* amplitude can be used to investigate the earthquake magnitude by the RTM. This approach is probably only limited by seismic station distribution if all earthquakes are correctly located.

[12] Similar to Q_{Lg} being used as a proxy of crustal Q_β, the Q_{Pg} can be assumed to be a proxy of crustal Q_α. We apply a very similar data processing and inversion method to the *Pg* data as we do with the *Lg* data; while some parameters, such as the group velocity window, the geometrical spreading coefficient, the threshold of maximum inter-station distance, etc, have been revised to appropriate values for *Pg* [*Bao et al.*, 2011]. The calculated RTM Q_{Pg} tomographic map is strongly correlated with the RTM Q_{Lg} model (Figure 2b) with high attenuation regions throughout most of the north and northeastern TP and low attenuation regions surrounding the TP. We observe differences in the relative attenuation structure between *Pg* and *Lg* in part of Qiangtang Terrane that may indicate strong crustal heterogeneity causing different degrees of scattering attenuation effects on *Pg* and *Lg*.

5. Conclusion

[13] Among various methods used to measure crustal Q, the RTM appears to be the most reliable. The estimation of site terms using the RTM in this study indicates that the site response is probably dependent on change of topography or sediment thickness. We observe a linear relationship between estimated logarithmic source terms and earthquake magnitudes M_L when $3 \le M_L \le 7$. We create high-resolution (for $1° \times 1°$ to $2° \times 2°$ anomalies) Q_{Lg} and Q_{Pg} models of eastern TP and adjacent areas using the RTM. The Q_{Lg} and Q_{Pg} tomographic models show strong lateral variations in the eastern TP and adjacent areas. The very low Q values observed in northwestern SGFB may suggest a hot crust, which could be related to high strain rate.

[14] **Acknowledgments.** We are grateful to all members of the INDEPTH-IV and NETS teams, the Seismotectonic group at Peking University, and the IRIS DMC for collecting seismic data. We thank Daniel McNamara and an anonymous reviewer for helpful feedback greatly improving this paper. The research in this study is supported by the National Science Foundation of China under grants 40520120222 and 40821062, and the National Science Foundation of the United States under grants EAR-0634903, EAR-0409589, and EAR-0409870.

[15] The Editor thanks Daniel McNamara and an anonymous reviewer for their assistance in evaluating this paper.

References

Bao, X., E. Sandvol, E. Zor, S. Sakin, R. Mohamad, R. Gök, R. Mellors, T. Godoladze, G. Yetirmishli, and N. Türkelli (2011), Pg attenuation tomography within the northern Middle East, *Bull. Seismol. Soc. Am.*, in press.

Brune, J. N. (1970), Tectonic stress and the spectra of seismic shear waves from earthquakes, *J. Geophys. Res.*, *75*, 4997–5009, doi:10.1029/JB075i026p04997.

Chun, K.-Y., G. F. West, R. J. Kokoski, and C. Samson (1987), A novel technique for measuring Lg attenuation results from eastern Canada between 1 to 10 Hz, *Bull. Seismol. Soc. Am.*, *77*, 398–419.

Fan, G., and T. Lay (2003), Strong Lg wave attenuation in the northern and eastern Tibetan Plateau measured by a two-station/two-event stacking method, *Geophys. Res. Lett.*, *30*(10), 1530, doi:10.1029/2002GL016211.

Ford, S. R., D. S. Dreger, K. Mayeda, W. R. Walter, L. Malagnini, and W. S. Phillips (2008), Regional attenuation in Northern California: A comparison of five 1D Q methods, *Bull. Seismol. Soc. Am.*, *98*, 2033–2046, doi:10.1785/0120070218.

Hacker, B. R., E. Gnos, L. Ratschbacher, M. Grove, and M. McWilliams (2000), Hot and dry deep crustal xenoliths from Tibet, *Science*, *287*, 2463–2466, doi:10.1126/science.287.5462.2463.

Hanks, T. C., and H. Kanamori (1979), A moment magnitude scale, *J. Geophys. Res.*, *84*, 2348–2350, doi:10.1029/JB084iB05p02348.

Holt, W. E., N. Chamot-Rooke, X. Le Pichon, A. J. Haines, B. Shen-Tu, and J. Ren (2000), Velocity field in Asia inferred from Quaternary fault slip rates and Global Positioning System observations, *J. Geophys. Res.*, *105*, 19,185–19,209, doi:10.1029/2000JB900045.

Jemberie, A. L., and C. A. Langston (2005), Site amplification, scattering, and intrinsic attenuation in the Mississippi embayment from coda waves, *Bull. Seismol. Soc. Am.*, *95*, 1716–1730, doi:10.1785/0120040203.

Kennett, B. L. N. (1989), On the nature of regional seismic phases—I. Phase representations for Pn, Pg, Sn, Lg, *Geophys. J. Int.*, *98*, 447–456, doi:10.1111/j.1365-246X.1989.tb02281.x.

Klemperer, S. L. (2006), Crustal flow in Tibet: Geophysical evidence for the physical state of Tibetan lithosphere, and inferred patterns of active flow, in *Channel Flow, Ductile Extrusion and Exhumation in Continental Collision Zones*, edited by R. D. Law, *Geol. Soc. Spec. Publ.*, *268*, 39–70, doi:10.1144/GSL.SP.2006.268.01.03.

Li, Y., H. Yao, Q. Liu, J. Chen, R. D. van der Hilst, S. Li, H. Huang, B. Guo, J. Wang, and S. Qi (2010), Phase velocity array tomography of Rayleigh waves in western Sichuan from ambient seismic noise, *Chin. J. Geophys.*, *53*(1), 842–852, doi:10.3969/j.issn.0001-5733.2010.04.009.

McKenzie, D., and K. Priestley (2008), The influence of lithosphere thickness variations on continental evolution, *Lithos*, *102*, 1–11, doi:10.1016/j.lithos.2007.05.005.

McNamara, D. E., T. J. Owens, and W. R. Walter (1996), Propagation characteristics of *Lg* across the Tibetan Plateau, *Bull. Seismol. Soc. Am.*, *86*, 457–469.

Mitchell, B. J. (1995), Anelastic structure and evolution of the continental crust and upper mantle from seismic surface wave attenuation, *Rev. Geophys.*, *33*, 441–462, doi:10.1029/95RG02074.

Moya, A., and K. Irikura (2003), Estimation of site effects and *Q* factor using a reference event, *Bull. Seismol. Soc. Am.*, *93*, 1730–1745, doi:10.1785/0120020220.

Nabelek, P. I., A. G. Whittington, and A. M. Hofmeister (2010), Strain heating as a mechanism for partial melting and ultrahigh temperature metamorphism in convergent orogens: Implications of temperature-dependent thermal diffusivity and rheology, *J. Geophys. Res.*, *115*, B12417, doi:10.1029/2010JB007727.

Paige, C. C., and M. A. Saunders (1982), LSQR: An algorithm for sparse linear equations and sparse lest squares, *Trans. Math. Software*, *8*, 43–71, doi:10.1145/355984.355989.

Phillips, W. S., H. E. Hartse, S. R. Taylor, and G. E. Randall (2000), 1 Hz Lg Q tomography in central Asia, *Geophys. Res. Lett.*, *27*, 3425–3428, doi:10.1029/2000GL011482.

Reese, C. C., R. R. Rapine, and J. F. Ni (1999), Lateral variation of Pn and Lg attenuation at the CDSN station LSA, *Bull. Seismol. Soc. Am.*, *89*, 325–330.

Shin, Y. H., H. Xu, C. Braitenberg, J. Fang, and Y. Wang (2007), Moho undulations beneath Tibet from GRACE-integrated gravity data, *Geophys. J. Int.*, *170*, 971–985, doi:10.1111/j.1365-246X.2007.03457.x.

Su, F., K. Aki, T. Teng, Y. Zeng, S. Koyanagi, and K. Mayeda (1992), The relation between site amplification factor and surficial geology in central California, *Bull. Seismol. Soc. Am.*, *82*, 580–602.

Wald, D. J., and T. I. Allen (2007), Topographic slope as a proxy for seismic site conditions and amplification, *Bull. Seismol. Soc. Am.*, *97*, 1379–1395, doi:10.1785/0120060267.

Xie, J. (2002), Lg Q in the eastern Tibetan Plateau, *Bull. Seismol. Soc. Am.*, *92*, 871–876, doi:10.1785/0120010154.

Xie, J., and B. J. Mitchell (1990), Attenuation of multiphase surface waves in the Basin and Range province, part I: Lg and Lg coda, *Geophys. J. Int.*, *102*, 121–137, doi:10.1111/j.1365-246X.1990.tb00535.x.

Yang, Y., et al. (2010), Rayleigh wave phase velocity maps of Tibet and the surrounding regions from ambient seismic noise tomography, *Geochem. Geophys. Geosyst.*, *11*, Q08010, doi:10.1029/2010GC003119.

X. Bao and E. Sandvol, Department of Geological Sciences, University of Missouri, 101 Geology Bldg., Columbia, MO 65203, USA. (xbqzb@mail.missouri.edu; sandvole@missouri.edu)

Y. J. Chen, Institute of Theoretical and Applied Geophysics, School of Earth and Space Sciences, Peking University, Beijing 100871, China. (johnyc@pku.edu.cn)

T. Hearn and J. Ni, Department of Physics, New Mexico State University, MSC 3D, Las Cruces, NM 88003, USA. (thearn@nmsu.edu; jni@nmsu.edu)

Y. Shen, Graduate School of Oceanography, University of Rhode Island, 203 Horn Bldg., South Ferry Road, Narragansett, RI 02882, USA. (yshen@gso.uri.edu)